Research Square

Preprints are preliminary reports that have not undergone peer review.
They should not be considered conclusive, used to inform clinical practice,
or referenced by the media as validated information.

Fabrication and Characterization of Cellulose-based Hydrogels with Polymerizable Ionic Liquids for 3D Printing Applications

Keito Matsumoto
Sophia University
Tamao Saito
Sophia University
Yuko Takeoka
Sophia University
Masahiro Rikukawa
Sophia University
Masahiro Yoshizawa-Fujita
masahi-f@sophia.ac.jp

Sophia University

Research Article

Keywords: Direct ink writing, Biomass processing, Radical polymerization, Semi-interpenetrating polymer network, Shear-thinning ink

Posted Date: November 11th, 2026

DOI: https://doi.org/10.21203/rs.3.rs-10696310/v1

License: This work is licensed under a Creative Commons Attribution 4.0 International License.
Read Full License

Additional Declarations: No competing interests reported.

Fabrication and Characterization of Cellulose-based Hydrogels with Polymerizable Ionic Liquids for 3D Printing Applications

Keito Matsumoto, Tamao Saito, Yuko Takeoka, Masahiro Rikukawa, Masahiro Yoshizawa-Fujita*

Department of Materials & Life Sciences
Sophia University
7-1 Kioi-cho, Chiyoda-ku, Tokyo 102-8554, Japan
Phone: 03-3238-3498
Fax: 03-3238-4198
masahi-f@sophia.ac.jp

Abstract: Cellulose is an abundant, sustainable, and low-cost material; however, its strong intra- and intermolecular hydrogen bonding makes it insoluble in water and most organic solvents. Ionic liquids such as 1-butyl-3-methylimidazolium chloride ([C_4mim]Cl) have therefore been widely used to dissolve and process cellulose under mild conditions. In this study, cellulose-based hydrogels were prepared using cellulose, [C_4mim]Cl, and an ionic liquid (IL) monomer. The crystallinity and chemical structure of the hydrogels were characterized, and their water content and mechanical properties were evaluated as a function of cellulose concentration. Incorporation of polymerized ionic liquid (PIL) into the cellulose network significantly enhanced the mechanical strength compared to conventional cellulose hydrogels. Antibacterial activity was assessed by the disk diffusion method. In addition, the rheological behavior of cellulose solutions was investigated, and the resulting inks were successfully applied to 3D printing. The cellulose/PIL hydrogels exhibited high water content, improved mechanical strength, and excellent printability. Although [C_4mim]Cl effectively inhibited Escherichia coli growth, this antibacterial effect was lost after washing the hydrogels. These results demonstrate that cellulose/PIL hydrogels are promising structural platforms for functional materials, with tunable properties suitable for future specialized and potentially biomedical applications.

Keywords: Cellulose • Ionic Liquids • 3D Printing • Photopolymerization • Hydrogels

Abbreviations:[C_4mim]Cl: 1-butyl-3-methylimidazolium chloride; IL: Ionic liquid; PIL: Polymerized ionic liquid; [C_4mpyr][OH]/H_2O: Aqueous solution of N-butyl-N-methylpyrrolidinium hydroxide; CO_2: Carbon dioxide; DIW: Direct ink writing; XRD: X-ray diffraction; S–S curves: Stress–strain curves; *E. coli*: Escherichia coli; *S. epidermidis*: Staphylococcus epidermidis; G': Storage modulus; G": Loss modulus; DP: Degree of polymerization; HOMPP: 2-hydroxy-2-methylpropiophenone

Introduction

Cellulose is the primary structural component of plant cell walls and the most abundant natural polymer on Earth (Pinkert 2009). Cellulose-derived biomass can be produced without reliance on fossil fuels, thereby reducing greenhouse gas emissions (Gui 2013). Furthermore, because it can be utilized as a non-edible resource that does not compete with food or feed, cellulose has attracted considerable attention as an environmentally friendly and sustainable material (Söyler 2018). Cellulose is a linear polymer consisting of β-glucose units connected by 1,4-glycosidic linkages, and it forms extensive intra- and intermolecular hydrogen bonding (McNamara 2015). Consequently, cellulose is insoluble in water and most common organic solvents, as these solvents are unable to break its strong hydrogen-bonding network (Lindman 2010).

Conventional solvents for cellulose include N-methylmorpholine N-oxide (NMMO), sodium hydroxide, and aqueous zinc chloride ($ZnCl_2$) solutions. The Lyocell process, which employs NMMO for the non-derivatizing dissolution of cellulose, has been commercialized and enables the dissolution of up to 20 wt% cellulose in a short time. However, NMMO exhibits limited

thermal stability, and side reactions have been reported to degrade the performance of the resulting hydrogels (Wang 2016). Sodium hydroxide is an inexpensive solvent for cellulose; however, it requires processing at −10 °C and its dissolution capacity is restricted to about 5 wt% (Liebert 2010). Aqueous $ZnCl_2$ solutions have attracted attention for their ease of preparation and low cost; nevertheless, they exhibit poor cellulose solubility and require high temperatures and prolonged treatment (Shu 2022; Zhang 2019). Therefore, conventional cellulose solvents pose significant environmental challenges and exhibit inherent limitations in dissolution capacity.

In recent years, ionic liquids have gained significant attention as promising solvents for cellulose because they can dissolve cellulose under mild conditions. Ionic liquids are salts with melting points below 100 °C (Seiler 2020). Composed of cations and anions, their strong electrostatic interactions confer low volatility and non-flammability, making them recyclable and environmentally benign solvents (Cassity 2013; Ferreira 2012). By tuning the combination of cations and anions, a broad spectrum of physicochemical properties can be achieved (Lefroy 2021). Consequently, ionic liquids have been widely investigated across diverse fields, ranging from battery electrolytes to bioscience applications (Ohno 2019). Among these, biomass refining is a notable application area. Ionic liquids can dissolve cellulose, and studies have shown that the electron-donating ability of the anion correlates with cellulose dissolution efficiency (Zhao 2013). For example, $[C_4mim]Cl$ can dissolve up to 10 wt% cellulose at 100 °C without activation or pretreatment (Swatloski 2002). Similarly, 1-ethyl-3-methylimidazolium methyl phosphonate, synthesized via a one-pot process, dissolves 4 wt% cellulose at 25 °C (Fukaya 2008). Furthermore, an aqueous solution of N-butyl-N-methylpyrrolidinium hydroxide ($[C_4mpyr][OH]/H_2O$) containing 50 wt% water can dissolve up to 20 wt% cellulose at room temperature (Matsui 2025).

Cellulose hydrogel preparation methods can be broadly classified into two categories: chemical crosslinking and physical crosslinking. Chemical crosslinking involves forming covalent bonds between cellulose chains using crosslinking agents such as epichlorohydrin or glutaraldehyde. In contrast, physical crosslinking induces gelation by re-establishing hydrogen bonds during cellulose regeneration, wherein cellulose is first dissolved in a solvent and then precipitated in a nonsolvent such as water. For instance, cellulose hydrogels can be prepared by dissolving cellulose in $[C_4mim]Cl$ followed by washing with water to remove the ionic liquid (Swatloski 2002). Additionally, a carbon dioxide-assisted method has been reported. When cellulose dissolved in $[C_4mpyr][OH]/H_2O$ is exposed to a CO_2 atmosphere, hydroxide ions (OH^-) react with CO_2 to form carbonate (CO_3^{2-}) and bicarbonate (HCO_3^-) ions. This anionic transformation lowers the solution pH from 14 to 9, leading to a loss of cellulose solubility and subsequent gelation, thereby producing a cellulose hydrogel (Matsui 2025). Hydrogels obtained via this approach have garnered significant attention as sustainable materials.

Hydrogels possess high water absorption and retention capabilities, and their biodegradability and biocompatibility make them attractive for diverse applications, including wound dressings, drug delivery systems, tissue engineering, bioimaging, wearable sensors, and 3D printing inks (Xue 2025). However, cellulose hydrogels often exhibit inadequate mechanical properties. One strategy to enhance their mechanical strength is the use of crosslinking agents; nevertheless, conventional approaches employing toxic crosslinkers are complex and offer limited

performance improvements. Chenglong Zou et al. demonstrated the fabrication of multiscale silk fiber–cellulose composites by incorporating silk fibers into a solution of microcrystalline cellulose and [C4mim]Cl. Compared with conventional regenerated cellulose, these composites showed a 123.06% increase in tensile strength and a 91.68% increase in Young's modulus (Zou 2024). Similarly, Michael A. Smirnov et al. reported that introducing acrylic acid into a solution of bacterial cellulose and either [C4mim]Cl or choline chloride, followed by UV-induced radical polymerization, resulted in poly(acrylic acid) grafting onto cellulose nanofiber surfaces. This modification significantly improved the mechanical strength of the resulting material (Smirnov 2021).

3D printing is an additive manufacturing technique that creates three-dimensional structures by sequentially depositing material layers according to a computer-generated 3D model (Xiong 2020). Commercialized in 1987 by 3D Systems, this technology is now employed not only for prototyping but also for producing functional end-use products. Several printing methods have been developed, including inkjet 3D printing, fused deposition modeling, direct ink writing (DIW), and micro-extrusion bioprinting. Among these, DIW is particularly promising for biomaterial applications due to its ability to process a wide variety of materials (Li 2017). In DIW, high-viscosity inks are extruded layer by layer to build three-dimensional structures. However, during printing, each deposited layer is influenced by gravity and surface tension, which can compromise shape fidelity. Consequently, post-printing stabilization processes are essential for maintaining the integrity of printed structures.

The use of cellulose and ionic liquids as 3D printing inks represents a promising strategy for advancing sustainability through environmentally friendly material development. Moreover, this approach is expected to address a key challenge in DIW—maintaining structural integrity after extrusion—by leveraging the high viscosity of cellulose. Mano Govindharaj et al. developed a DIW ink composed of alginate, collagen derived from fish skin, and cellulose microfibers obtained from banana stems, demonstrating its potential as a wound dressing material (Govindharaj 2024). The integration of cellulose-based materials with 3D printing technology is anticipated to enable personalized wound dressings tailored to the size and geometry of individual wounds, thereby improving the quality of healthcare.

The purpose of this study is to systematically elucidate the physical properties of cellulose-based composite materials with polymerizable ionic liquids for 3D printing applications. Cellulose-based gel materials were prepared using cellulose, [C_4mim]Cl as the cellulose solvent, and an ionic liquid monomer structurally analogous to [C_4mim]Cl, which served as a polymer precursor. By tailoring the chemical structure of the cellulose solvent to resemble that of the ionic liquid monomer, improved miscibility without phase separation is expected. Accordingly, [C_4mim]Cl was selected due to its structural similarity to the ionic liquid monomer, rather than using ionic liquids such as [C_2mim]Cl or [C_2mim]Ac, which possess higher cellulose dissolution capacity. It is hypothesized that the in situ photopolymerization of the IL monomer within the entangled cellulose matrix would lead to the formation of a semi-interpenetrating polymer network. The synergistic effect of cellulose entanglement and the formation of ionic polymer composites is anticipated to significantly improve the mechanical strength of the resulting hydrogels. Furthermore, the suitability of a cellulose solution containing an ionic liquid monomer for 3D printing was also evaluated.

Results and Discussion

Evaluation of Cellulose Structure

The crystallinity of cellulose was assessed using X-ray diffraction (XRD) analysis. Fig. 1(a) presents the chemical structure of cellulose, [C4mim]Cl, and IL monomer. After photopolymerization, Composite-1-12.5 formed a soft, elastic yellow gel, with the coloration likely originating from trace lignin components present in Avicel® and the ionic liquid (see Fig. 1(b)) (Seiler 2021). Following washing with distilled water to remove the ionic liquid, Composite-2-12.5 transformed into a semi-transparent white gel (see Fig. 1(c)). Subsequent freeze-drying yielded Composite-3-12.5 as a hard, dense white solid (see Fig. 1(d)). Fig. S1 shows the XRD patterns of Avicel® cellulose prior to dissolution in [C4mim]Cl, Composite-1-12.5 after dissolution, and Composite-3-12.5 obtained by freeze-drying after 24 h of washing with distilled water. Native Avicel® cellulose exhibited diffraction peaks at 15.6° and 22.3°, corresponding to the (110) and (200) planes, respectively (Gong 2017). In contrast, Composite-1-12.5 displayed no distinct diffraction peaks, indicating that dissolution in [C4mim]Cl disrupts intra- and intermolecular hydrogen bonding, leading to an amorphous structure. For Composite-3-12.5, diffraction peaks appeared at 12.5° and 20.7°, corresponding to the (110) and (110) planes, respectively (French 2014; Hong 2021). These results suggest that removing the ionic liquid by washing promotes cellulose recrystallization, accompanied by a structural transition from parallel-packed cellulose I to antiparallel-packed cellulose II.

Based on these results, changes in the crystalline structure of cellulose were observed, and the emergence of cellulose II, as is commonly observed upon regeneration, was confirmed. The crystallinity index (see Experimental section) of cellulose before dissolution was 59.9%, whereas after regeneration, it was 56.9%. These results suggest that the dissolution of cellulose in [C4mim]Cl disrupted both intramolecular and intermolecular hydrogen bonds. Although the complete removal of [C4mim]Cl was not quantitatively verified, several experimental observations indicate that the 24 h washing process was effective. First, the yellow coloration of Composite-1, likely due to trace impurities in the IL, completely disappeared, yielding the semi-transparent white appearance of Composite-2 and 3. Second, the XRD results showing the transition to cellulose II provide physical evidence of solvent removal, as this recrystallization is triggered by the displacement of [C4mim]Cl from the cellulose chains. Most importantly, the functional evidence from antibacterial tests (discussed below) further supports the substantial removal of the IL

Water Content

To examine the influence of cellulose concentration on water retention properties, the water content of the hydrogels was measured. Fig. 2 illustrates the relationship between water content and the number of immersion cycles for Composite-2-*y* (*y* = 5.0, 7.5, 10.0, 12.5). As shown in the Figure, the water contents of Composite-2-*y* (*y* = 5.0, 7.5, 10.0, 12.5) were 1933%, 1383%, 1015%, and 838%, respectively. Given that the optimal water content for wound dressings is reported to range

from 100–900% (Morgado 2015), the hydrogel prepared at 12.5 wt% cellulose (Composite-2-12.5) exhibits suitable water retention for such applications. A clear trend of decreasing water content with increasing cellulose concentration was observed. This behavior is attributed to densification of the cellulose network at higher concentrations, which reduces pore size and limits space for water retention (Satani 2020). Similar trends have been reported for cellulose hydrogels prepared via epichlorohydrin-mediated chemical crosslinking and those formed in NaOH/urea solutions, in which increased cellulose concentration enhances intermolecular hydrogen bonding and chain entanglement, thereby strengthening the network and reducing swelling capacity (Seiler 2021; Chang 2020). For hydrogels prepared by CO^{2-}-induced crosslinking, water contents of 950% and 776% were observed at cellulose concentrations of 5 wt% and 10 wt%, respectively (Matsui 2025). Collectively, these findings confirm that water content decreases with increasing cellulose concentration across all systems, although the preparation method significantly influences water absorption behavior.

Regardless of cellulose concentration, the water content decreased progressively with each cycle of freeze-drying and re-immersion. This observation indicates that dehydration disrupts the cellulose network structure, which cannot be completely restored upon rehydration. During freeze-drying, additional hydrogen bonds form between cellulose chains, leading to a more compact and aggregated network. As a result, even after re-immersion in water, the hydrogel does not fully recover its original (pre-dried) water content (Park 2024). Similar behavior has been reported for nanostructured cellulose II gels produced via the Lyocell process, where freeze-dried samples exhibited lower water retention compared to undried samples. This reduction is attributed to the formation of extra hydrogen bonds during drying, which strengthens the network and limits its capacity to absorb water (Beaumont 2017).

Mechanical Properties

Compression tests were performed to assess the mechanical properties of the hydrogels. Fig. 3 illustrates the maximum compressive strength of Composite-2-*y* (*y* = 5.0, 7.5, 10.0, 12.5) prepared with varying cellulose concentrations and the corresponding stress–strain (*S*–*S*) curves are shown in Fig. S2. For each condition, three hydrogel samples were tested in triplicate, and the average values are reported with error bars representing the standard deviation (n = 3). The maximum compressive strength of Composite-2-5.0 was 2.24 MPa, while those of Composite-2-*y* (*y* = 7.5, 10.0, 12.5) were 3.20, 3.60, and 4.68 MPa, respectively. The observed increase in compressive strength with higher cellulose concentration is attributed to the formation of a denser cellulose network, which enhances the hydrogel's mechanical integrity (Zhang 2025). For comparison, cellulose hydrogels prepared by dissolving cellulose in [P14][OH]/H_2O, crosslinking with CO_2, and washing for 24 h exhibited a maximum compressive strength of 1.2 MPa (Matsui 2025), whereas those crosslinked with epichlorohydrin showed only 0.07 MPa (Seiler 2021). The hydrogels developed in this study demonstrate superior mechanical strength relative to these conventional systems, likely due to composite formation with ionic liquid polymers. This significant reinforcement is attributed to the formation of a semi-interpenetrating polymer network through the in-situ photopolymerization of the IL monomer within the dissolved cellulose matrix. The structural

similarity between [C4mim]Cl and the IL monomer ensure high miscibility, preventing phase separation and allowing for a uniform distribution of PIL chains throughout the cellulose network. Furthermore, the XRD results (Fig. S1) indicate that the removal of [C4mim]Cl during the washing process triggers the recrystallization of cellulose from cellulose I to cellulose II. This structural transition likely "locks" the PIL chains within the regenerating cellulose network, facilitating effective stress transfer and resulting in the observed high compressive strength of 4.68 MPa, which is orders of magnitude higher than that of gels formed by conventional chemical or physical crosslinking. Notably, a double-network hydrogel composed of bacterial cellulose and gelatin (0.8 wt%) achieved a compressive strength of 7.4 MPa with a swelling ratio of 5.8 (Gong 2004). In contrast, Composite-2-12.5 exhibited a swelling ratio of 9.7, indicating that the hydrogels developed here combine excellent water retention with mechanical strength comparable to advanced hydrogel systems.

Antibacterial Test

Antibacterial test against *S. epidermidis*, a Gram-positive bacterium, and *E. coli*, a Gram-negative bacterium and a potentially hazardous pathogen in burn wounds (Busch 2000) was performed on Composite-*x*-12.5 samples (x = 1-3). Fig. 4 presents the results of antibacterial tests for *S. epidermidis*. Fig. S3 presents the results of antibacterial tests for *E. coli.* Each condition was tested in triplicate, and the mean inhibition zone diameter was used as the representative value. The inhibition zone, comparable to that produced by an ampicillin-impregnated paper disk, was observed around Composite-1-12.5, whereas no inhibition zones were detected for Composite-2-12.5 and Composite-3-12.5. The inhibition zone diameter for Composite-1-12.5 was 46.00 mm against *S. epidermidis* and 16.00 mm against *E. coli.* Composite-1 contained cellulose, the IL polymer, and [C4mim]Cl; Composite-2 consisted of cellulose, the IL polymer, and water; and Composite-3 comprised cellulose and the IL polymer only. These findings indicate that the antibacterial activity observed for Composite-1-12.5 is attributable to [C4mim]Cl. Thus, [C4mim]Cl exhibits antibacterial properties, whereas the IL polymer alone does not. The absence of inhibition zones in the washed samples (Composite-2 and 3) serves as a functional indicator that [C4mim]Cl, which is responsible for the antibacterial activity, was reduced to levels below the minimum inhibitory concentration. This reinforces the conclusion that the washing process effectively removed the bulk of the [C4mim]Cl solvent from the hydrogel network.

Effect of Cellulose Amount on Rheological Properties

Fig. 5 shows the viscosity curves of cellulose composites measured using a rheometer. At low shear rates, the viscosities of Composite-0-*y* (y = 5.0, 7.5, 10.0, 12.5) were 1.6×10^3, 3.8×10^3, 6.6×10^3, and 3.5×10^4 Pa·s, respectively. Viscosity increased with cellulose concentration, attributable to the greater number of polymer chains at higher concentrations, which enhances chain entanglement and a denser intermolecular network (Ahokas 2024; Zheng 2019). Across all concentrations, viscosity decreased with increasing shear rate, demonstrating shear-thinning behavior (Govindharaj 2024). At low shear rates, cellulose chains are randomly entangled,

producing high viscosity. As shear rate increases, the applied force stretches and aligns the chains along the flow direction, thereby facilitating their motion and reducing viscosity (Ahokas 2024). This shear-thinning property is critical for 3D printing because it enables smooth ink extrusion through the nozzle (Poulin 2021).

Strain sweep measurements were performed on inks with varying cellulose concentrations. Fig. 6 shows the storage modulus (G') and loss modulus (G") as functions of shear strain. The loss modulus reflects the viscous component of viscoelastic behavior and is indicative of liquid-like properties, whereas the storage modulus represents the elastic component and corresponds to solid-like characteristics. For 3D printing applications, inks must exhibit a yield point (G' = G") and maintain a high storage modulus. In the absence of applied stress, G' exceeds G", signifying a solid-like state that preserves internal structure. Under applied stress, such as extrusion pressure during printing, G" surpasses G', and the ink transitions to a fluid-like state, enabling smooth extrusion through the nozzle. If G" dominates even in the absence of strain, the extruded ink will lack shape fidelity, thereby compromising the printed structure. Therefore, achieving both a distinct yield point and a high storage modulus is essential for ensuring structural integrity after extrusion (Govindharaj 2024; Hausmann 2020).

For Composite-0-5.0, the loss modulus exceeded the storage modulus across the entire shear strain range, and no yield point was detected. This behavior indicates the absence of a stable internal network formed by cellulose chains in the solution (Zheng 2019). Consequently, Composite-0-5.0 is unsuitable for use as a 3D printing ink. In contrast, Composite-0-*y* (*y* = 7.5, 10.0, 12.5) exhibited yield points at shear strains of 6.9%, 21.7%, and 10.1%, respectively. At low shear strains, the storage modulus exceeded the loss modulus, suggesting that these formulations possess a stable network structure capable of resisting shear stress, likely due to physical entanglement and intermolecular interactions among cellulose chains (Jiang 2021). Based on their yield point behavior and high storage modulus, Composite-0-*y* (*y* = 7.5, 10.0, 12.5) are considered suitable for 3D printing applications. For comparison, gels composed of TEMPO-oxidized cellulose nanofibrils (TOCNF) crosslinked with metal cations maintain a storage modulus greater than the loss modulus regardless of shear rate, resulting in a stable gel state that cannot be extruded (Mietner 2021). These findings highlight that, unlike TOCNF gels, the present ink formulation combines structural stability with extrudability, making it applicable for 3D printing.

Frequency sweep measurements were performed on inks with varying cellulose concentrations. Fig. 7 presents the storage modulus (G') and loss modulus (G") as functions of angular frequency. For Composite-0-*y* (*y* = 7.5, 10.0, 12.5), G' consistently exceeded G" across the entire frequency range, indicating that cellulose chains are densely entangled and exhibit solid-like (elastic) behavior rather than fluid-like (viscous) behavior (Zheng 2019). Moreover, G' showed minimal frequency dependence, suggesting a stable network structure and high gel stability. In contrast, for Composite-0-5.0, G" exceeded G', and both moduli increased with frequency, indicating low gel stability and poor structural integrity. Similar trends have been reported for TEMPO-oxidized CNF hydrogels, in which G' remains higher than G" across the frequency range, indicating a stable gel state (Mietner 2021). Likewise, inks formulated from bacterial cellulose,

acrylic acid, and choline chloride or [C4mim]Cl exhibit G' > G" across all frequencies, reinforcing the importance of a dominant storage modulus for 3D printing applications (Smirnov 2021).

Effect of Cellulose Amount on Shape by 3D Printing

Fig. 8 shows the results of 3D-printed lattice structures. Composite-1-5.0 exhibited low ink viscosity, and the printed structures failed to maintain their shape under gravity. This is likely due to the low elastic modulus, which provided insufficient strength to support the structure post-printing (Jiang 2021). In contrast, lattice structures were successfully fabricated using Composite-1-7.5 and Composite-1-10.0, while Composite-1-12.5 demonstrated the highest formability. To assess formability, line widths of the printed lattices were measured, and the spreading ratio (actual-width/nozzle-width) is shown in Fig. S4. With a nozzle width of 0.41 mm, the measured line widths were 2.5, 1.9, 1.2, and 0.71 mm for increasing cellulose concentrations, indicating reduced spreading and improved shape fidelity at higher concentrations. Composite-1-12.5 produced the most precise 3D structure. Consistent with previous reports, increasing cellulose concentration increases ink viscosity, thereby improving formability (Kosan 2008). Similar trends have been observed in inks containing cellulose acetate sulfate: low-viscosity inks spread laterally and collapsed, whereas an optimal concentration of 4 wt% provided sufficient viscosity for stable structures (Park 2024). In this study, the use of ionic liquids enabled dissolution at high cellulose concentrations, and the incorporation of IL monomers significantly improved mechanical strength, achieving compressive strengths of 3.20, 3.60, and 4.68 MPa, compared with 0.048 MPa for Ca^{2+}-crosslinked systems (Park 2024). Although both approaches are applicable to 3D printing, the present formulation exhibits superior mechanical performance owing to its high cellulose content and integration of IL polymers.

Experimental Section

Materials

Microcrystalline cellulose (Avicel® PH-101) was purchased from Sigma-Aldrich and vacuum-dried at 80 °C for 12 h prior to use. The degree of polymerization (DP) is reported to range from 166 to 350 (Doelker 1987). 1-Methylimidazole (>99.0%), 1-chlorobutane (>99.0%), 4-bromo-1-butanol (>80.0%), Methacryloyl chloride (>90.0%) were purchased from Tokyo Chemical Industry Co., Ltd, and were used as received. Dichloromethane, Super Dehydrated (>99.5%), Triethylamine (>99.0%), Acetonitrile (>99.5%), Ethyl acetate (>99.5%) were purchased from FUJIFILM Wako Pure Chemical Corp., and were used as received.

Synthesis of 1-Butyl-3-Methylimidazolium Chloride ($[C_4mim]Cl$)

1-Methylimidazole (49.69 g, 0.6090 mol) and 1-chlorobutane (62.01 g, 0.6699 mol) were mixed and stirred under a nitrogen atmosphere at 70 °C for 72 h. Upon completion of the reaction, the resulting pale yellow viscous liquid was transferred to a separatory funnel and washed three times with ethyl

acetate. The obtained sample was then dried using a rotary evaporator, followed by vacuum drying, yielding a pale yellow viscous liquid.

Synthesis of 1-(4-Methacryloyloxybutyl)-3-Methylimidazolium Bromide (IL monomer)

The IL monomer was synthesized according to the previous report (Murakami 2007). 4-Bromo-1-butanol (8.46 g, 55.3 mmol) and methacryloyl chloride (6.00 g, 57.4 mmol) were dissolved in dichloromethane (50 mL). Under an argon atmosphere, triethylamine (12 mL, 86.1 mmol) was added dropwise to the mixture at 0 °C, and the mixed solution was stirred for 4 h, producing a turbid liquid. After filtration to remove triethylamine hydrochloride, dichloromethane (50 mL) was added to the filtrate, and the organic layer was washed three times each with water and saturated brine. The obtained sample (4-bromobutyl methacrylate) was dried over magnesium sulfate, and the solvent was removed using a rotary evaporator. The product was then collected after vacuum drying (7.71 g, Yield: 63.5%).

1-Methylimidazole (1.59 g, 19.1 mmol) and 4-bromobutyl methacrylate (4.04 g, 18.3 mmol) were dissolved in acetonitrile (10 mL) and stirred at 85 °C under an argon atmosphere for 16 h. The resulting product was precipitated by the addition of diethyl ether, collected by vacuum filtration, and dried under reduced pressure to obtain the desired compound (3.32 g, Yield: 59.8%).

Preparation of Cellulose Solution

A given amount (0.150, 0.225, 0.300, and 0.375 g) of Avicel cellulose dried at 80 °C for 24 h was mixed with [C_4mim]Cl (3 g, 17.18 mmol) and stirred at 100 °C for 24 h to dissolve the cellulose. The dissolution time of 24 h was determined based on a previous report (Murakami 2007). Subsequently, IL monomer (0.10 g, 0.330 mmol) and a photopolymerization initiator, 2-hydroxy-2-methylpropiophenone (HOMPP) (0.005 g, 0.006 mmol), were added into the mixture.

Fabrication of Composite Materials

After returning the synthesized material to room temperature, it was placed in a Petri dish and exposed to 365 nm UV light for 20 min to induce photopolymerization, resulting in stabilization (Composite-1). Composite-1 was then washed with distilled water for 24 h to remove [C_4mim]Cl, yielding a cellulose hydrogel (Composite-2). In this study, a 24 h washing process was adopted. While precise quantification of residual IL remains to be addressed in future work, its practical removal was verified based on physical and functional assessments. The distilled water in Composite-2 was removed by freeze-drying to obtain the fabricated structure (Composite-3). Freeze-drying was performed using an FDU-1200 freeze dryer (EYELA, Japan). The composites are denoted as "Composite-*x*-*y*", where *x* represents the composite number (0 - 3), and *y* indicates the weight ratio (wt%) of cellulose to the IL. The sample before photopolymerization is referred to as Composite-0.

X-ray Diffraction (XRD) Analysis

XRD analysis was performed to investigate the crystalline structure of cellulose and the fabricated cellulose hydrogel. Measurements were conducted at room temperature using monochromatic Cu Kα radiation (λ=1.5418 Å) on the fully automated multipurpose X-ray diffractometer, SmartLab, manufactured by Rigaku. The crystallinity index of cellulose and composite-3-12.5 was calculated using equation (1).

$$\mathrm{CrI} = \frac{I_{total} - I_{am}}{I_{total}} \times 100\% \ (1)$$

Here, I_{total} represents the intensity of the main peak, and I_{am} represents the minimum intensity between the main peak and the secondary peak.

Water Content Ratio of Cellulose Hydrogels

To evaluate the water retention stability, freeze-drying and re-immersion process was repeated seven times. After each freeze-drying cycle, samples were immersed in water at 22 °C for 5 h, and the water content was measured. Excess surface water on the hydrogel (Composite-2) was gently removed using filter paper, and the swollen hydrogel weight (W_{wet}) was measured. Subsequently, the hydrogel was freeze-dried, and the dried weight (W_{dry}) of Composite-3 was recorded. For each condition, three samples were tested in triplicate, and the average values are reported with error bars representing the standard deviation (n = 3). The water content of the hydrogel was calculated using Equation (2).

$$\text{Moisture content ratio} = \frac{W_{wet} - W_{dry}}{W_{dry}} \times 100\% \ (2)$$

Mechanical Properties of Cellulose Hydrogel

To evaluate the mechanical properties of the obtained hydrogel, a compression test was conducted using an Imada compression testing machine (MX2-500 N). The test was performed at room temperature with a crosshead speed of 10 mm/min. Cylindrical samples with a height of 0.4 cm and a radius of 1.3 cm were used. The elongation ratio of the cellulose hydrogel was determined from the displacement of the crosshead during the measurement.

Antibacterial Test

The antibacterial properties of composites-1, 2, and 3 were evaluated. Each composite was molded into a disk shape and placed on agar plates inoculated with *E. coli* and *S. epidermidis*. To confirm the validity of the antibacterial test, a paper disk impregnated with ampicillin, a standard antibacterial agent, and another disk impregnated with water, a non-antibacterial control, were placed on the same plates. Antibacterial activity was assessed by measuring the diameter of the inhibition zones formed around the samples. The presence of a clear inhibition zone around the ampicillin-impregnated disk and the absence of one around the water-impregnated disk confirmed that the antibacterial test was performed correctly.

Rheological Measurements

The rheological properties of the cellulose solution were evaluated to investigate its rheological behavior. Measurements were conducted using an Anton Paar MCR302e rheometer equipped with a P-PTD220 plate-type Peltier temperature control unit and a CP25-2 cone-plate geometry (diameter: 25 mm, cone angle: 1°). To prevent corrosion of the aluminum stage of the P-PTD220, a stainless steel protective plate was used. Viscosity curve measurements were performed over a shear strain range of 0.01% to 1000%, strain sweep measurements were conducted over a shear strain range of 0.01% to 1000%, and frequency sweep measurements were carried out over an angular frequency range of 0.1 rad s^{-1} to 100 rad s^{-1}.

3D Printing

The cellulose solution was loaded into a syringe and extruded into a cartridge. It was then connected to the printhead of a 3D printer equipped with a sterile standard conical bioprinting nozzle and extruded under an applied air pressure of 200 kPa at room temperature (20 °C) to fabricate a lattice structure (30 × 30 × 1 mm) with three layers at a printing speed of 1.00 mm/s. The printed structure was subsequently exposed to 365 nm UV light for 20 min using the UV lamp of the 3D printer to obtain the printed construction. A BIOX 3D bioprinter (CELLINK) was used for fabrication.

Conclusion

In this study, the crystallinity, chemical structure, water content, mechanical strength, and antibacterial properties of cellulose hydrogels were systematically evaluated. Additionally, rheological behavior was analyzed, and 3D printing was performed using the prepared inks to assess printability. XRD analyses confirmed that Avicel® cellulose dissolved in [C_4mim]Cl underwent a crystalline transition from cellulose I to cellulose II during regeneration, while retaining the fundamental β-(1→4)-glycosidic backbone characteristic of Avicel® cellulose. Increasing cellulose concentration reduced water content; notably, Composite-2-12.5 exhibited a water content of 838%, within the optimal range for wound dressing applications (100–900%). Compressive strength also increased with cellulose concentration, and the resulting hydrogels exhibited superior mechanical performance compared to previously reported cellulose-based hydrogels, likely due to the reinforcing effect of the IL polymer. Antibacterial tests revealed that [C_4mim]Cl exhibited antibacterial activity, whereas the IL polymer did not. Rheological measurements demonstrated shear-thinning behavior, and Composite-0-*y* (*y* = 7.5, 10.0, 12.5) exhibited properties suitable for 3D printing inks. Composite-1-12.5 successfully produced well-defined lattice structures, indicating that higher viscosity improved printability. Collectively, these results suggest that cellulose/IL polymer hydrogels developed in this study serve as versatile 3D-printable scaffolds with robust mechanical integrity. Although detailed biological assessments—such as cytotoxicity and hemocompatibility—are necessary to confirm their safety for clinical use, the current findings provide a significant step toward designing cellulose-based functional platforms for potential high-end applications.

Author contributions Keita Matsumoto: conceptualization, methodology, formal analysis, investigation, resources, writing – original draft, visualization. Tamao Saito: data curation, supervision. Yuko Takeoka: data curation, supervision. Masahiro Rikukawa: data curation, supervision. Masahiro Yoshizawa-Fujita: conceptualization, methodology, data curation,writing – review & editing, visualization, supervision, project administration, funding acquisition.

Funding This work was supported by a Sophia University Special Grant for Academic Research.

Data availability This manuscript does not report data generation or analysis.

Declarations

Conflict of interest There are no conflicts to declare.

References

Ahokas P, Mäkelä M, Jaiswal A, Khakalo A, Harlin A (2024) Controlling the rheology of cellulose dissolved in 4-methylmorpholine N-oxide and tensile properties of precipitated cellulose films via mixture design. Cellulose 31:10403−10421.https://doi.org/10.1007/s10570-024-06214-y

Beaumont M, König J, Opietnik M, Potthast A, Rosenau T (2017) Drying of a cellulose II gel: effect of physical modification and redispersibility in water. Cellulose 24:1199–1209. https://doi.org/10.1007/s10570-016-1166-9

Busch NA, Zanzot EM, Loiselle PM, Carter EA, Allaire JE, Yarmush ML, Warren HS (2000) A Model of Infected Burn Wounds Using Escherichia coli O18:K1:H7 for the Study of Gram-Negative Bacteremia and Sepsis. Infect Immun 68:3349–3351. https://doi.org/10.1128/iai.68.6.3349-3351.2000

Cassity CG, Mirjafari A, Mobarrez N, Strickland KJ, O'Brien RA, Davis JH Jr (2013) Ionic liquids of superior thermal stability. Chem Commun 49:7590. https://doi.org/10.1039/c3cc44118k

Chang C, Zhang L, Zhou J, Zhang L, Kennedy JF (2010) Structure and properties of hydrogels prepared from cellulose in NaOH/urea aqueous solutions. Carbohydr Polym 82:122–127. https://doi.org/10.1016/j.carbpol.2010.04.033

Doelker E, Gurny R, Schurz J, Janosi A, Matin N (1987) Degrees of Crystallinity and Polymerization of Modified Cellulose Powders for Direct Tableting. Powder Technol 52:207–213.

Ferreira AF, Simões PN, Ferreira AGM (2012) Quaternary phosphonium-based ionic liquids: Thermal stability and heat capacity of the liquid phase. J Chem Thermodyn 45:16–27. https://doi.org/10.1016/j.jct.2011.08.019

French A (2014) Idealized powder diffraction patterns for cellulose polymorphs. Cellulose 21:885-896. https://doi.org/10.1007/s10570-013-0030-4

Fukaya Y, Hayashi K, Wada M, Ohno H (2008) Cellulose dissolution with polar ionic liquids under mild conditions: required factors for anions. Green Chem 10:44–46. https://doi.org/10.1039/b713289a

Gong JP, Katsuyama Y, Kurokawa T, Osada Y (2004) High Mechanical Strength Double-Network Hydrogel with Bacterial Cellulose. Adv Funct Mater 14:318–322. https://doi.org/10.1002/adfm.200305197

Gong J, Li J, Xu J, Xiang Z, Mo L (2017) Research on cellulose nanocrystals produced from cellulose sources with various polymorphs. RSC Adv 7:33486. https://doi.org/10.1039/c7ra06222b

Govindharaj M, Al Hashimi N, Soman SS, Zhou J, AlAwadhi S, Vijayavenkataraman S (2024) 3D-bioprinted tri-layered cellulose/collagen-based drug-eluting fillers for the treatment of deep tunneling wounds. Bio-Des Manuf 7:938–954. https://doi.org/10.1007/s42242-024-00305-2

Gui Z, Zhu H, Gillette E, Han X, Rubloff GW, Hu L, Lee SB (2013) Natural cellulose fiber as substrate for supercapacitor. ACS Nano 7:6037–6046. https://doi.org/10.1021/nn401818t

Hausmann MK, Siqueira G, Libanori R, Kokkinis D, Neels A, Zimmermann T, Studart AR (2020) Complex-Shaped Cellulose Composites Made by Wet Densification of 3D Printed Scaffolds. Adv Funct Mater 30:1904127. https://doi.org/10.1002/adfm.201904127

Hong T, Yin J-Y, Nie S-P, Xie M-Y (2021) Applications of Infrared Spectroscopy in Polysaccharide Structural Analysis: Progress, Challenge and Perspective. Food Chem X 12:100168. https://doi.org/10.1016/j.fochx.2021.100168

Jiang J, Oguzlu H, Jiang F (2021) 3D printing of lightweight, super-strong yet flexible all-cellulose structure. Chem Eng J 405:126668. https://doi.org/10.1016/j.cej.2020.126668

Kosan B, Michels C, Meister F (2008) Dissolution and forming of cellulose with ionic liquids. Cellulose 15:59–66. https://doi.org/10.1007/s10570-007-9160-x

Lefroy KS, Murray BS, Ries ME (2021) Rheological and NMR Studies of Cellulose Dissolution in the Ionic Liquid BmimAc. J Phys Chem B 125:8205–8218. https://doi.org/10.1021/acs.jpcb.1c02848

Li VC-F, Dunn CK, Zhang Z, Deng Y, Qi HJ (2017) Direct Ink Write (DIW) 3D Printed Cellulose Nanocrystal Aerogel Structures. Sci Rep 7:8018. https://doi.org/10.1038/s41598-017-07771-y

Liebert T (2010) Cellulose Solvents – Remarkable History, Bright Future. ACS Symp Ser 1033:3–54. https://pubs.acs.org/doi/full/10.1021/bk-2010-1033.ch001

Lindman B, Karlström G, Stigsson L (2010) On the mechanism of dissolution of cellulose. J Mol Liq 156:76–81.

Matsui A, Putri DA, Thomas ML, Takeoka Y, Rikukawa M, Yoshizawa-Fujita M (2025) A Simple Regeneration Process Using a CO^{2-}-Switchable-Polarity Solvent for Cellulose Hydrogels. ChemSusChem 18:e202401848. https://doi.org/10.1002/cssc.202401848

McNamara JT, Morgan JLW, Zimmer J (2015) A Molecular Description of Cellulose Biosynthesis. Annu Rev Biochem 84:895–921. https://doi.org/10.1146/annurev-biochem-060614-033930

Mietner JB, Jiang X, Edlund U, Saake B, Navarro JRG (2021) 3D printing of a bio-based ink made of cross-linked cellulose nanofibrils with various metal cations. Sci Rep 11:6461. https://doi.org/10.1038/s41598-021-85865-4

Morgado PI, Aguiar-Ricardo A, Correia IJ (2015) Asymmetric membranes as ideal wound dressings: An overview on production methods, structure, properties and performance relationship. J Membr Sci 490:139–151. https://doi.org/10.1016/j.memsci.2015.04.06

Murakami M, Kaneko Y, Kadokawa J (2007) Preparation of cellulose-polymerized ionic liquid composite by in-situ polymerization of polymerizable ionic liquid in cellulose-dissolving solution. Carbohydr Polym 69:378–381. https://doi.org/10.1016/j.carbpol.2006.12.002

Ohno H, Yoshizawa-Fujita M, Kohno Y (2019) Functional Design of Ionic Liquids: Unprecedented Liquids that Contribute to Energy Technology, Bioscience, and Materials Sciences. Bull Chem Soc Jpn 92:852–881. https://doi.org/10.1246/bcsj.20180401

Park S, Sharmin T, Cho S-M, Kelley SS, Shirwaiker RA, Park S (2024) Single-Component Cellulose Acetate Sulfate Hydrogels for Direct Ink Writing 3D Printing. Biomacromolecules 25:5889–5901. https://doi.org/10.1021/acs.biomac.4c00578

Pinkert A, Marsh KN, Pang S, Staiger MP (2009) Ionic Liquids and Their Interaction with Cellulose. Chem Rev 109:6712–6728. https://doi.org/10.1021/cr9001947

Poulin A, Aeby X, Siqueira G, Nyström G (2021) Versatile carbon-loaded shellac ink for disposable printed electronics. Sci Rep 11:23701. https://doi.org/10.1038/s41598-021-03075-4

Satani H, Kuwata M, Shimizu A (2020) Simple and environmentally friendly preparation of cellulose hydrogels using an ionic liquid. Carbohydr Res 494:108054. https://doi.org/10.1016/j.carres.2020.108054

Seiler ERD, Takeoka Y, Rikukawa M, Yoshizawa-Fujita M (2020) Development of a novel cellulose solvent based on pyrrolidinium hydroxide and reliable solubility analysis. RSC Adv 10:11475. https://doi.org/10.1039/d0ra01486a

Seiler ERD, Koyama K, Iijima K, Saito T, Takeoka Y, Rikukawa M, Yoshizawa-Fujita M (2021) Simple and Fast One-Pot Cellulose Gel Preparation in Aqueous Pyrrolidinium Hydroxide Solution–Cellulose Solvent and Antibacterial Agent. Polymers 13:1942 https://doi.org/10.3390/polym13121942

Söyler Z, Onwukamike KN, Grelier S, Grau E, Cramail H, Meier MAR (2018) Sustainable succinylation of cellulose in a CO^{2-}based switchable solvent and subsequent Passerini 3-CR and Ugi 4-CR modification. Green Chem 20:214–222. https://doi.org/10.1039/c7gc02577g

Shu L, Zhang X-F, Wang Z, Yao J (2022) Structure reorganization of cellulose hydrogel by green solvent exchange for potential plastic replacement. Carbohydr Polym 275:118695. https://doi.org/10.1016/j.carbpol.2021.118695

Smirnov MA, Fedotova VS, Sokolova MP, Nikolaeva AL, Elokhovsky VY, Karttunen M (2021) Polymerizable Choline- and Imidazolium-Based Ionic Liquids Reinforced with Bacterial Cellulose for 3D-Printing. Polymers 13:3044. https://doi.org/10.3390/polym13183044

Swatloski RP, Spear SK, Holbrey JD, Rogers RD (2002) Dissolution of Cellulose with Ionic Liquids. J Am Chem Soc 124:4974–4975. https://doi.org/10.1021/ja025790m

Wang S, Lu A, Zhang L (2016) Recent advances in regenerated cellulose materials. Prog Polym Sci 53:169–206. http://dx.doi.org/10.1016/j.progpolymsci.2015.07.003

Xiong S (2020) Materials, Application Status and Development Trends of Additive Manufacturing Technology. Mater Trans 61:1191–1199. https://doi.org/10.2320/matertrans.MT-M2020023

Xue H, Zhu C, Wang Y, Gu Q, Shao Y, Jin A, Zhang X, Lei L, Li Y (2025) Stimulus-responsive cellulose hydrogels in biomedical applications and challenges. Mater Today Bio 32:101814. https://doi.org/10.1016/j.mtbio.2025.101814

Zhang X-F, Ma X, Hou T, Guo K, Yin J, Wang Z, Shu L, He M, Yao J (2019) Inorganic Salts Induce Thermally Reversible and Anti-Freezing Cellulose Hydrogels. Angew Chem Int Ed 58:7366–7370. https://doi.org/10.1002/anie.201902578

Zhang Y, Kobayashi K, Wada M (2025) Comparative analysis of the structures and properties of cellulose hydrogels prepared using different solvent systems. Cellulose 32:2337–2351. https://doi.org/10.1007/s10570-025-06437-7

Zhao Y, Liu X, Wang J, Zhang S (2013) Effects of anionic structure on the dissolution of cellulose in ionic liquids revealed by molecular simulation. Carbohydr Polym 94:723–730. https://doi.org/10.1016/j.carbpol.2013.02.011

Zheng B, Harris C, Bhatia SR, Thomas MF (2019) Dissolution capacity and rheology of cellulose in ionic liquids composed of imidazolium cation and phosphate anions. Polym Adv Technol 30:1751–1758. https://doi.org/10.1002/pat.4607

Zou C, Lv J, Zhu K, Jiao Y, Rong J, Zhang W, He X, Pan Q, Zhang X, Hua X, Liu B (2024) Construction and 3D Printing of Multiscale Silk Fiber-Cellulose Composite Networks Based on Ionic Liquids. Adv Mater Technol 10:2400847. https://doi.org/10.1002/admt.202400847

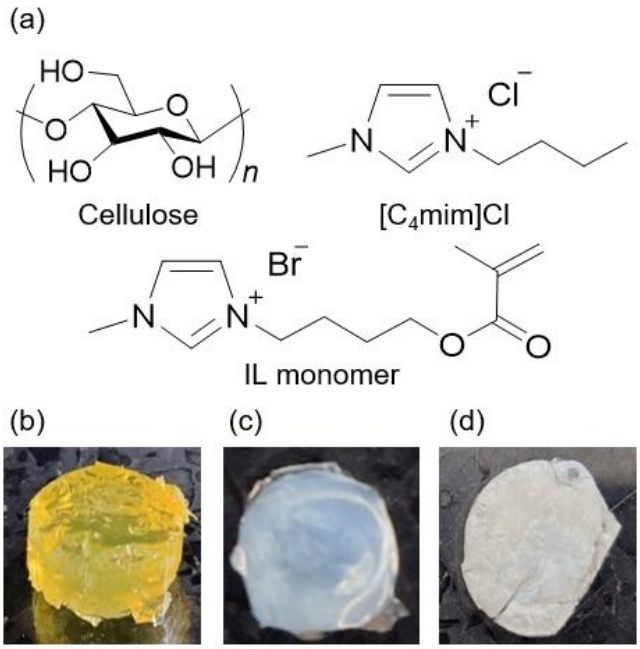


Fig. 1 (a) Chemical structure of cellulose, [C_4mim]Cl, and IL monomer, and photographs of cellulose composites: (b) Composite-1-12.5, (c) Composite-2-12.5, and (d) Composite-3-12.5

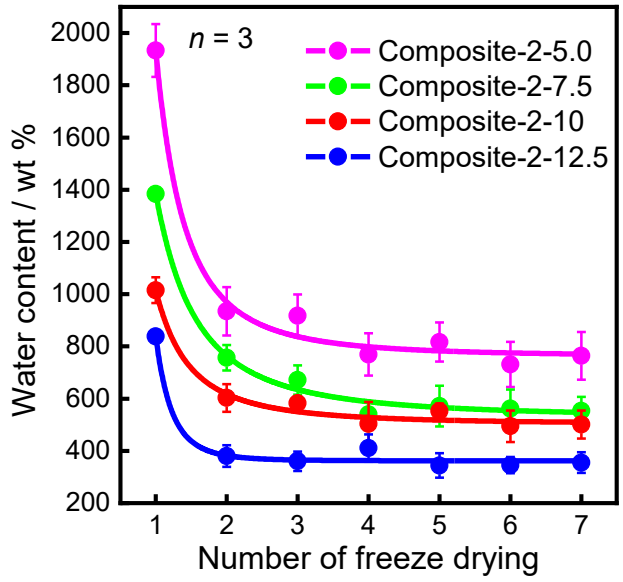


Fig. 2 Relationship between water content and number of freeze-drying cycles of cellulose hydrogels with various cellulose concentrations

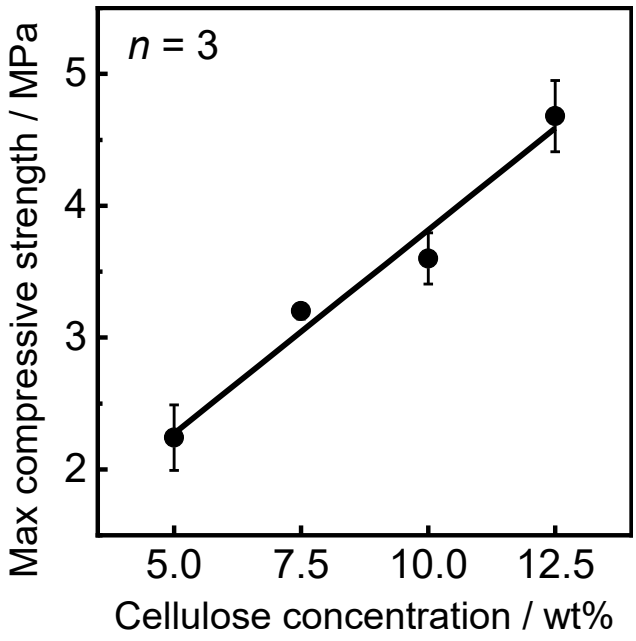


Fig. 3 Cellulose concentration dependence of maximum compressive strength for cellulose hydrogels

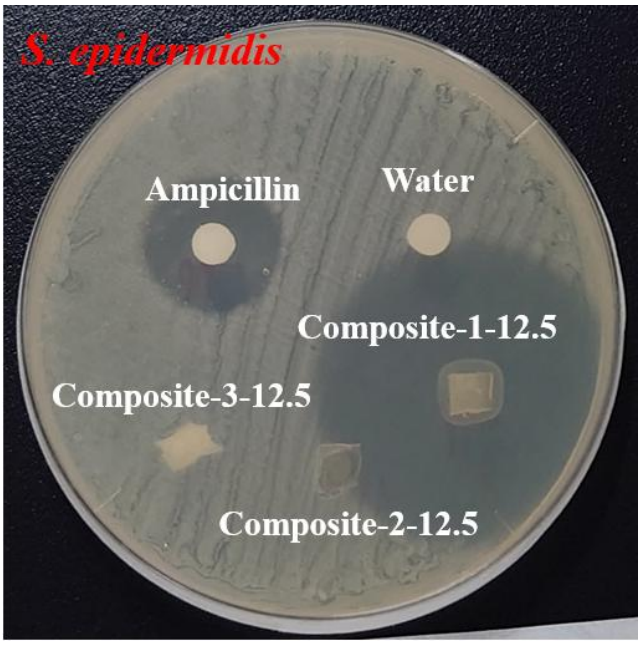


Fig. 4 Extract from the disk diffusion test. The antibacterial activity of cellulose composites at varying cellulose concentrations was evaluated against *S. epidermidis* after incubation at 37°C for 16 h

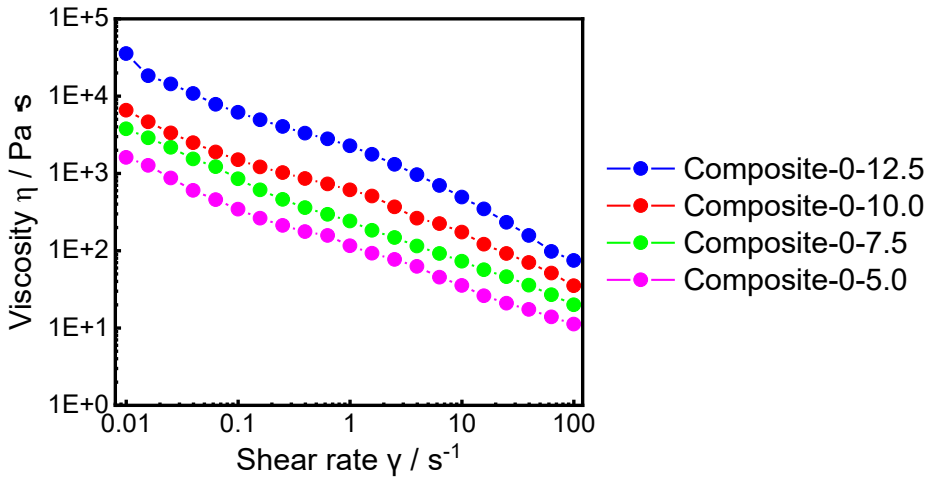


Fig. 5 Shear rate dependence of viscosity for various cellulose composites

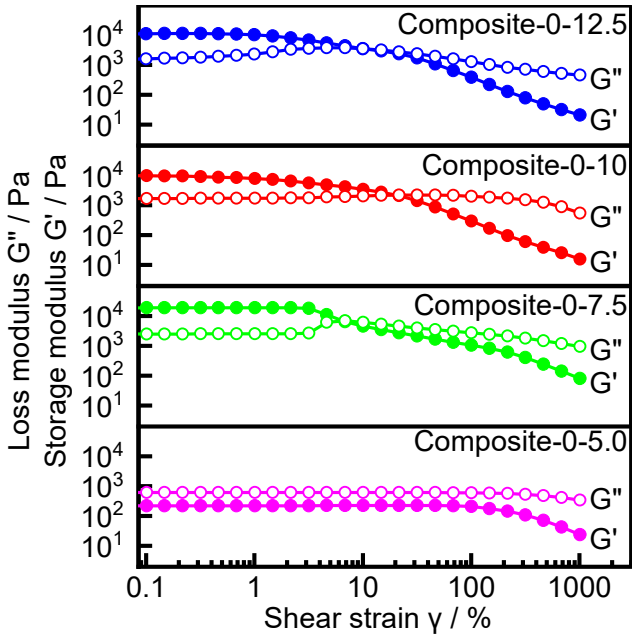


Fig. 6 Strain-sweep measurements of the loss and storage moduli at various cellulose concentrations

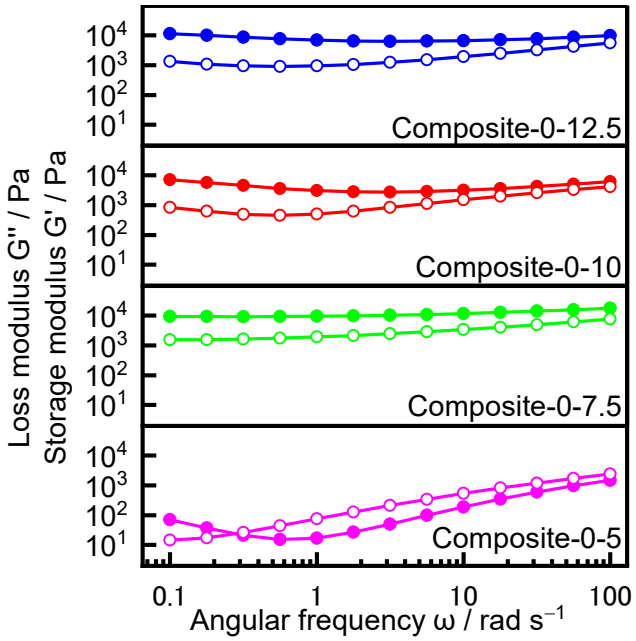


Fig. 7 Frequency sweep measurements of the loss and storage moduli at various cellulose concentrations

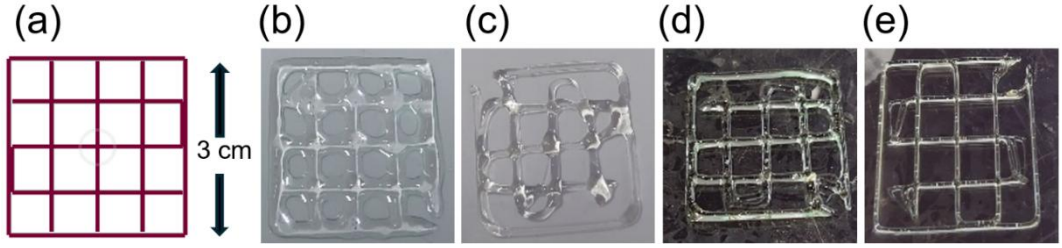


Fig. 8 Grid layers with various amounts of cellulose after 3D printing (a) model structure, (b) Composite-1-5.0, (c) Composite-1-7.5, (d) Composite-1-10.0, and (e) Composite-1-12.5

Supplementary Files

This is a list of supplementary files associated with this preprint. Click to download.

- SupportingInformationMatsumoto.docx